Canadian Chemical Transactions Year 2015 | Volume 3 | Issue 3 | Page 327-339

Research Article

DOI:10.13179/canchemtrans.2015.03.03.0223

High Photocatalytic Activity of Heterostrutured $InMoO_3$-Tio_2 Nanocomposite Material Under Natural Sun Light Irradiation

Jayaraman Kamalakkannan, Vijayaragavan Lenin Chandraboss, Selvaraj Prabha, Bala Karthikeyan and Sambandam Senthilvelan*

Department of Chemistry, Annamalai University, Annamalainagar 608 002, Tamilnadu, India.

Corresponding Author: Email: dr_senthilvel@yahoo.co.in

Received: *August 08, 2015* ***Revised:*** *September 23, 2015* ***Accepted:*** *October 3, 2015* ***Published:*** *October 11, 2015*

Abstract: Synthesize coupled semiconductor oxides development of $InMoO_3$ doped-TiO_2 nanocomposite material was synthesised by co-precipitation method and sonication technique. The synthesized nanomaterial was characterized using X-ray diffraction (XRD), high resolution scanning electron microscopy (HR-SEM) with EDX analysis, high-resolution transmission electron microscopy (HR-TEM), Fourier transform-infrared FT-IR spectrum and diffuses reflectance (DRS). The photocatalytic activity of $InMoO_3$ doped-TiO_2 nanomaterial was evaluated from the photodegradation of methyl green (MEG) under natural sun light irradiation and material was found to be stable and reusable.

Keywords: Heterostructured, HR-SEM, HR-TEM, Photocatalytic activity.

1. INTRODUCTION

Titanium dioxide is one of the most commonly used nanomaterials for photocatalytic applications suitable to its high chemical stability, low toxicity, low cost and brilliant oxidation properties [1, 2]. Titanium dioxide presents a moderately high electron–hole recombination rate due to its wide band gap energy (ca. 3.0 eV for rutile and 3.2 eV for anatase), and as a effect retards the photo activity of a multi module system, the extent of which also depends on the synthetic method used and its work [3].The effectiveness of photocatalytic reaction is mainly influenced by two viable processes, the passage rate of electrons and holes to the semiconductor's surface and the recombination rate of photoexcited charges [4]. To advanced quantum efficiency of the photocatalytic process, the inhibition of a fast recombination rate of active species is crucial [4,5]. Titanium dioxide has been widely used in photocatalytic processes due to being nontoxic, highly stable, excellent resistance to photocorrosion and low cost [6-8]. and inexpensive. Another semiconductor material with properties similar to those of Titanium dioxide is zinc oxide has established the most application after Titanium dioxide. Zinc oxide has been reported in several cases to have enhanced performance than Titanium dioxide for degradation of organic compounds [9,10]. This multimodal metal oxide system and depends on their compositions in the current year. The double

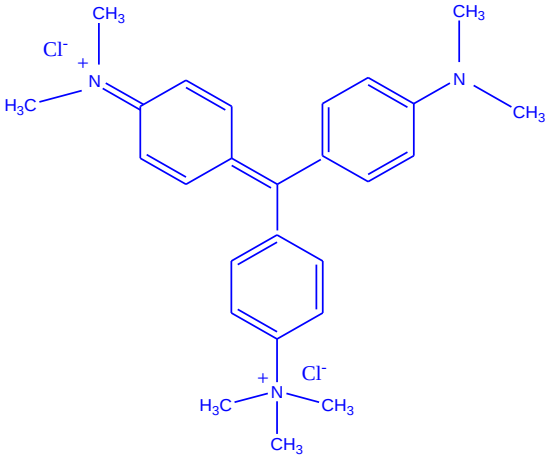

Figure 1. Chemical structure of Methyl green (MEG).

metal oxides such as for WO_3/ TiO_2 and TiO_2/MoO_3 have been in the main considered for their single chemical, physical and photocatalytic properties [11] Jiang Yin et al expose reported that $MCrO_4$ (M=Ba and Sr) had shows potential photocatalytic properties [12, 13]. MEG is one of the most common dying materials for silk, wood, and cotton material [14, 3]**.** The photocatalytic mineralization of industrial pollutants using modified metal oxides as photocatalyst is well established and has shown great value in the complete mineralization of industrial pollutants [15]. In this present work, $InMoO_3$ doped-TiO_2 nanocomposite material was synthesised by co-precipitation method and sonication technique. The synthesized nanomaterial was characterized using X-ray diffraction (XRD), high resolution scanning electron microscopy (HR-SEM) with EDX analysis, high-resolution transmission electron microscopy (HR-TEM), Fourier transform-infrared FT-IR spectrum and diffuses reflectance (DRS). The photocatalytic activity of $InMoO_3$ doped-TiO_2 nanomaterial was evaluated from the photodegradation of methyl green (MEG) under natural sun light irradiation and material was found to be stable and reusable.

2. EXPERIMENTAL

2.1. Materials

Tetra isopropyl orthotitanate, Ammonium heptamolybdate ($(NH_4)_6$ Mo_7O_{24}. $4H_2O$), Indium chloride, NH_3 solution, nitric acid-65%, methyl green (Fig.1) ($C_{26}H_{33}N_3Cl_2$) used are gift sample of TiO_2−P25 (80% anatase) and ethanol, the guaranteed reagents of Sigma Aldrich. Deionized water was used as a solvent throughout the experiment.

2.2. Synthesis of $InMoO_3$-TiO_2 nanomaterial

$InMoO_3$-TiO_2 was synthesised by co-precipitation method. The total synthesis was carried out in two steps as below.

Synthesis steps

Indium chloride and ammonium moliptate were first dissolved with deionized water. The as prepared $InCl_3$ solution was put in a beaker, and then slowly added Sodium tungstate until it is reached to

1:1 composite. Frequent magnetic stirring for 2 h was carried out to keep the reactant mixed uniformly. The pH of the solution was adjusted to 9 with ammonia solution. The obtained solution was placed in sonication for 40 mins to get a white precipitate. The precipitate was filtered and washed with distilled water for four to six times to remove the remaining Cl^- and Na^+ ions. Finaly the sample was dried at 100 ^{0}C for 2 h [16], the solution from I step and tetra isopropyl orthotitanate (0.1.5 mol/L was prepared by adding 50 ml of conductivity water to 450 ml produced a dispersed white precipitate. It was added to $InMoO_3$ with anhydrous ethanol as solvent under vigorous stiring for further 2 h, followed by sonication for 20 mins. The obtained precipitate was filtered and washed with distilled water and ethanol until alkali phases were removed from precipitation. Then the precipitate was collected and dried in oven at 100 ^{0}C for 12 h. The resulting powder was calcined at 500 ^{0}C for 3 h as shown in Sheme.1.

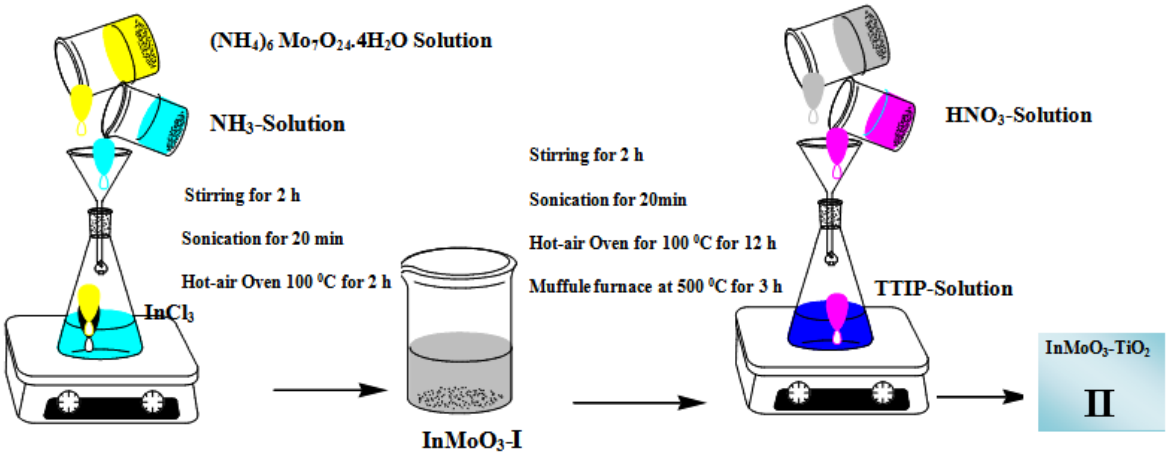

Scheme 1. Schematic representation for preparation of $InMoO_3$ -TiO_2 nanomaterial.

2.3. Characterization

X-ray diffraction (XRD) was recorded on the X'PERT PRO model X-ray diffractometer from Pan Analytical instruments operated at a voltage of 40 kV and a current of 30 mA with Cu Kα radiation The morphological observation of the prepared materials were made by Field-emission Scanning electron microscopy (HR-SEM) with elementary dispersive X-ray (EDX) analysis and it was carried out on a FEI Quanta FEG 200 instrument with EDX analyzer facility at 25 °C. The sample was prepared by placing a small quantity of the prepared material on a carbon coated copper grid and allowing the solvent to evaporate by high resolution transmission electron microscopy (HR-TEM), TECNAI G2 FEI F12 model. Fourier transform-infrared spectrum (FT-IR) was recorded using SHIMADZU FT-IR spectrometer in KBr pellet. The crystallinity was characterized by an UV-vis DRS and the direct band gap energy was analyzed by UV–visible (Shimadzu UV-1650 PC) spectrophotometer. Ultraviolet and visible (UV-vis) absorbance spectra were measured over a range of 800-200 nm with a Shimadzu UV-1650PC recording spectrometer using a quartz cell with 10 mm of optical path length.

2.4. Photodegradation Experiment.

The reaction out by using natural sun light photocatalytic degradation experiments were carried out under similar conditions on sunny days among 12 a.m. and 2 p.m. An open borosilicate glass reaction tube of 50 mL capacity, 40 cm height, and 20 mm diameter was used as the reaction container. In a typical

experiment aqueous suspensions of dye (40 mL, 1×10^{-4} M) and 0.150 g of the photocatalyst were loaded in reaction tubes. Prior to irradiation, the suspension At the time intervals of given irradiation time. The suspension was measured spectrophotometrically at 630 nm (MEG) dye within the Beer–Lambert law limit.

2.5. XRD analysis

XRD analysis of $InMoO_3$-TiO_2 nanocomposites material is shown in Fig. 2 respectively. It conforms that TiO_2 (JCPDS No. 21-1272), In and MoO_3 was present in (JCPDF no. 72-1184 and JCPDS card no. 05-0508) obtained. TiO_2 (101) and (211) crystal planes, In (101) and MoO_3 (040), (081) high crystal planes respectively, The samples are present in $InMoO_3$-TiO_2 exhibits a diffraction pattern of FCC crystal structure. The average crystalline size (L) of the particles have been calculated from the Debye–Scherrer formula, $L= 0.89\lambda / \beta \cos\theta$ where L is the crystalline size (in nm), l is the wavelength (in nm), b is the full width at half maximum intensity (FWHM-in radian), and u is the Bragg diffraction angle (θ). The average crystalline size of prepared material for average crystalline sizes of $InMoO_3$-TiO_2 nanomaterial is almost 33 nm.

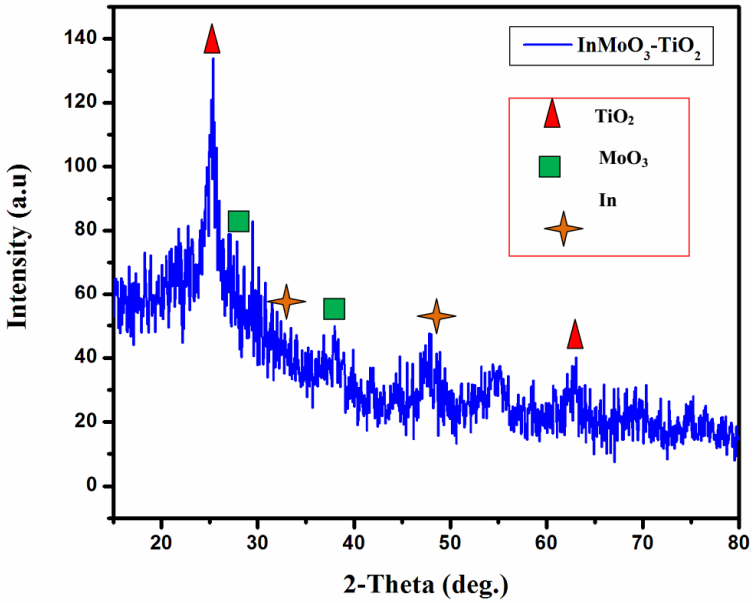

Figure 2. XRD analysis of prepared InMoO3-TiO2 nanomaterial.

2.6. SEM with EDX analysis

FE-SEM images of the prepared $InMoO_3$ doped-TiO_2 nanomaterial are shown in Fig.3a respectively. The FE-SEM image exposed that individual particles and shows the surface morphology as agglomerated various sized and spherical shaped particles. The FE-SEM images of the $InMoO_3$-TiO_2 shows an average particle size of 32 nm. EDX analysis conforms In, W, Ti and O are present in $InMoO_3$-TiO_2 nanomaterial are show in (Fig. 3 b)

2.7. HR-TEM analysis

(HR-TEM) measurements of $InMoO_3$ doped-TiO_2 at image are shown in Fig. 4.a. it is established that the presence of particles are depicted from the HR-TEM micrographs as well spherical shaped. The distances between the bonds were measured by analysis software. Fig.4 (b, c and d) represents an image profile, plot profile and particle size distribution (in nm). Fig. 4d shows an average particle size as about 90 nm by selected particle area highlighted Fig.4a.

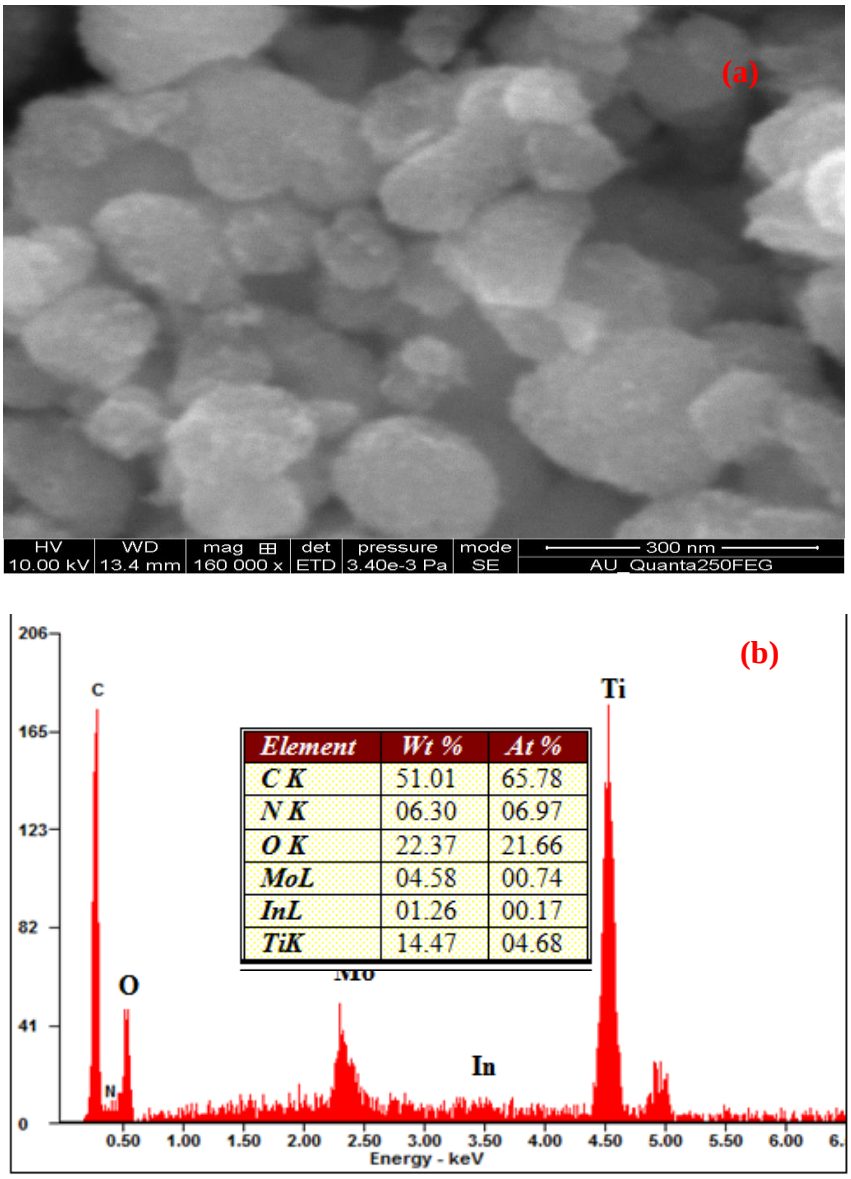

Figure 3. HR-SEM images of (a) $InMoO_3$ doped-TiO_2 nanomaterial (b) EDX analysis

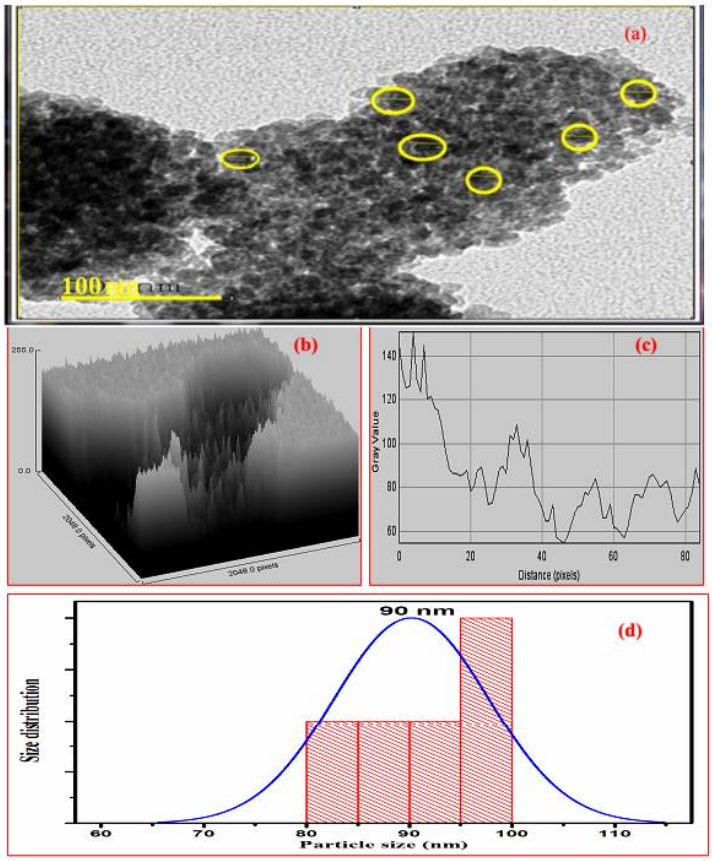

Figure 4. TEM images of InMoO3-TiO2 (a) particle distribution, (b) (b, c and d) surface plot, plot profile and particle size in selected area highlightedfig. 4(a).

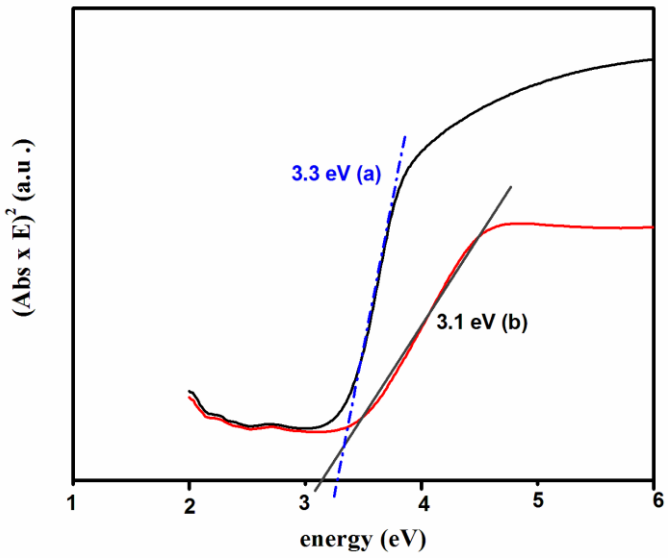

Figure 5. Tauc plots (a) TiO_2 and (b) $InMoO_3$-TiO_2 nanomaterial.

2.8. UV-Vis-DRS analysis

Fig. 5 (a-b) prepared TiO_2 and $InMoO_3$ Doped -TiO_2 in the direct band gap energy of synthesized nanomaterials has been resolute from the Tauc plots. The plots of absorbition Vs the photon energy (*hv*) give the band gap of the synthesized TiO_2 and $InMoO_3$ Doped -TiO_2 as 3.3 and 3.1 eV, correspondingly. The results $InMoO_3$-TiO_2 having low band gab energy high photocatalytic activity.

2.9. FT-IR analysis

The FTIR spectrum of $InMoO_3$- TiO_2 shows the peak positions are at 3700, 3250, 2929, 1629, 1460 1386 and 580 cm.-1 The band at 3700-3250 shows NH2 group aliphatic and aromatic group, 2929 shows C-H aliphatic group, 1629 is shows S-H2O bands, 1460 is due to O-H group, C=O that OR aromatic, C-N amine group and 580 cm_{-1} Ti-In-Mo-O-Ti bonds are show in Fig. 6.

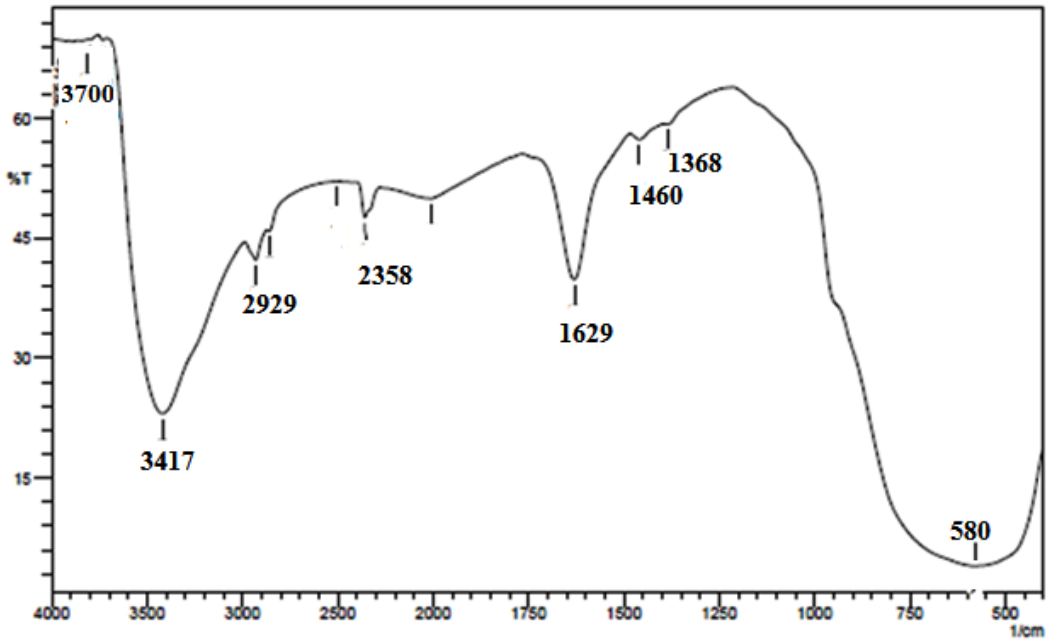

Figure 6. FT-IR spectrum of $InMoO_3$-TiO_2 nanomaterial.

3. Primary analysis of natural sun light irradiation.

The photodegradation process of MEG and natural sun light at 0 to 45 min irradiation spectra at 15 min time interval. The coloured solution of MEG was finally 45 min clear solution obtained in the presence of photocatalysts ($InMoO_3$- TiO_2) are illustrated in Fig. 7a. $InMoO_3$ Doped -TiO_2 material shows superior photocatalytic activity when compared undoped TiO_2 and TiO_2P25 in. Reaction of MEG undergoes % of degradation from 0, 35, 68, and 95% in the presence of $InMoO_3$ Doped -TiO_2 that TiO2 (0, 15, 33 and 65 %) and TiO_2 P25 (0, 9, 15 and 23 %) under natural sun light shown in Fig. 7b. Percentages of degradation at different pH from 3, 7, 9 and 11 for MEG dye. It is experimental that the degradation increases with an increase in pH up to 7 and then decreases under natural sun light irradiation as show in Fig.8.

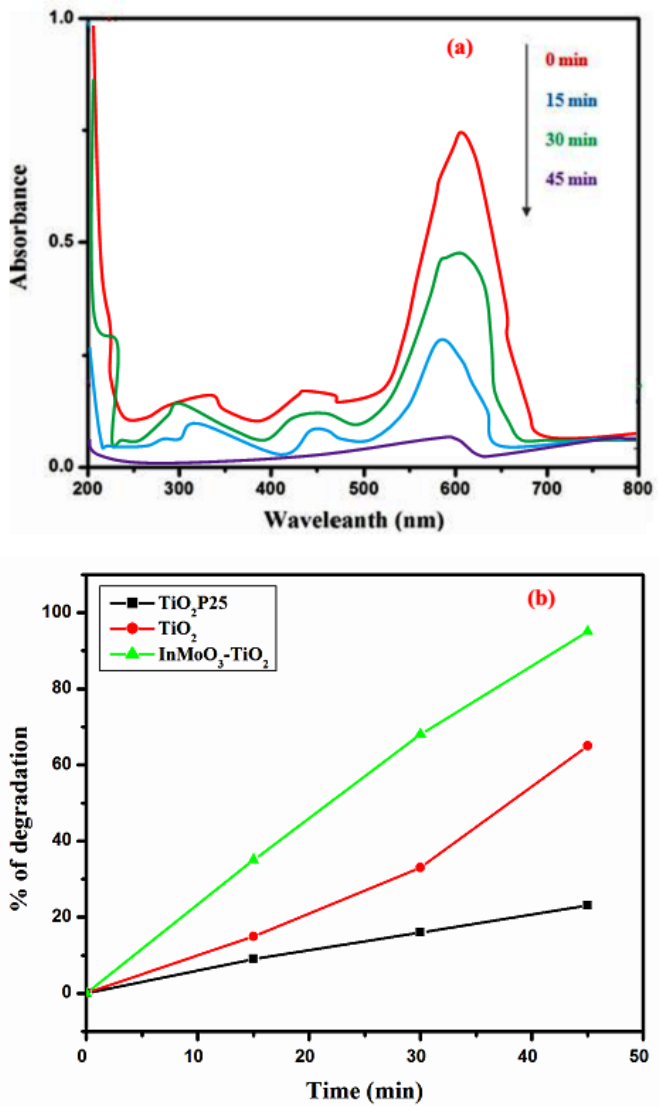

Figure 7. (a) InMoO3-TiO2 -Absorption spectra changes sun light irradiation and (b) Primary analysis of natural sun light irradiation.

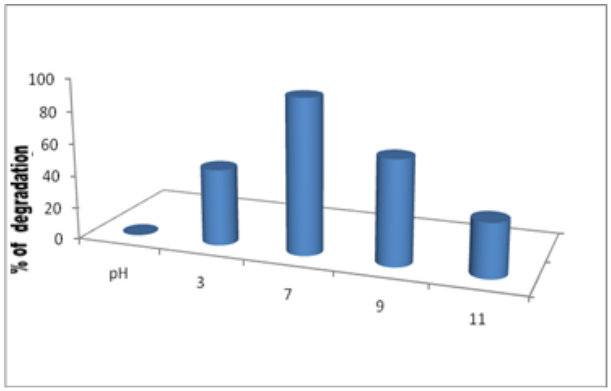

Figure 8. (a) Effect of pH prepared $InMoO_3$-TiO_2 on MEG dye under sun light irradiation.

3.1. Kinetics and quantum yield calculation

Kinetics study of MEG on prepared TiO_2 and $InMoO_3$ Doped -TiO_2 are calculated by using the pseudo-first-order kinetics model equation (1)

$$\ln (C_0/C_t) = Kapp^t \text{ ---------- (1)}$$

where $Kapp^t$ is the rate constant [min], C_0 is the initial concentration of MEG, and C_t is the concentration of MEG at reaction time (t), from the results in straight lain [17]. $InMoO_3$ Doped -TiO_2 showes the maximum degradation rate constant, around which is higher than that of TiO_2. The photodegradation rate constants (k′) of MEG dye in the monochromatic light source yields reaction quantum yield [18,19] by applied following eq- (2)

$$\Phi = \frac{k}{2.303\, I_{0,\lambda}\, \varepsilon_{D\lambda}\, l} \text{ ---------- (2)}$$

where Φ is the reaction of quantum yield (dimensionless), I_o is the light intensity of the incident light range at 200−800 nm range (1.381×10^{-6}), $\varepsilon_{D\lambda}$ is the molar absorptivity of MEG at 560 nm (3.192 X10 ^{4} cm^{-1} M^{-1}) and (l) is the path length of the reaction tube and is 0.24 m for 50 mL of irradiated solution. The final results of degradation quantum yields by, $InMoO_3$ Doped -TiO_2 and TiO_2 are 0.0821 and 0.0464 respectively as shown in Table 1. These results indicate that the quantum yield of the $InMoO_3$ Doped -TiO_2 process is elevated when compare to bare TiO_2 nanomaterial.

Table 1. Quantum yield of photocatalytic degradation of MEG in aqueous solution after 45 mins under solar-light-irradiation.

Catalyst	% degradation	Quantum Yield
TiO_2	65	0.0464
InMoO3-TiO_2	95	0.0821

3.2. Catalyst reusability

The stability and reusability of the $InMoO_3$ Doped -TiO_2 nnomaterial are achieved by repeating MEG degradation experiments for six more times. After each cycle the $InMoO_3$ Doped -TiO_2 photocatalysts were washed thoroughly with water, and a fresh solution of MEG was made before every run in the photoreactor. The complete degradation occurs in the 1st run (100 %), 2nd run (99 %), 3rd run (98.5 %), 4th run (98 %), 5th run (98 %) run 6th (98 %) runs as show in Fig.9. The result indicates that the prepared catalysts are stable and reusable. After the completion of the degradation process, the solution was tested for In^{3+} by leaching with Na_2S. There is no precipitation of In^{3+} S (black color) was found. As there is no further leaching of In^{3+}. So this responded material is non-hazardous for waste water treatment [20].

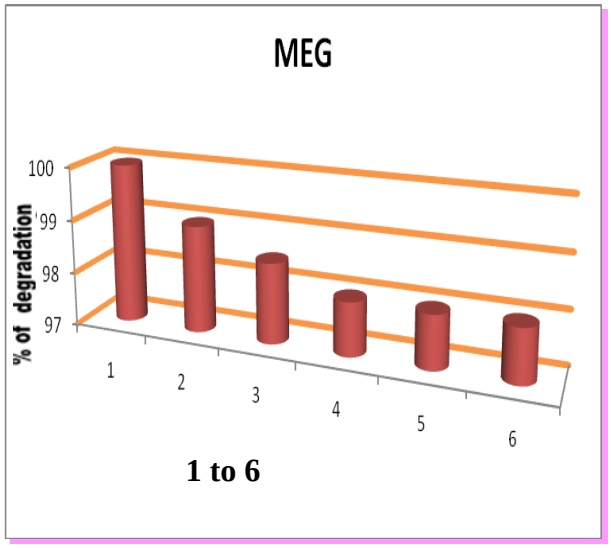

Figure 9. Reusability of $InMoO_3$-TiO_2 on MEG dye under sun light irradiation.

3.4. Mechanism

Sheme.2. Shows the general mechanism of the photodegradation by semiconducting oxide $InMoO_3$ Doped -TiO_2 towards MEG dye under active natural sun light irradiation. The energy of incident photons is superior to the band gap energy. The excitation of valence band (VB) electrons has advanced potential reactions. The incident of the photocatalytic surface area with enough energy leads to the array of a positive hole (hv^+) into the valence band and an electron (e−) through the conduction band (CB). The hole in the valence band reacts with the surface H_2O molecule to generate hydroxyl radicals which reacts with the MEG dye molecule to degrade the dye.

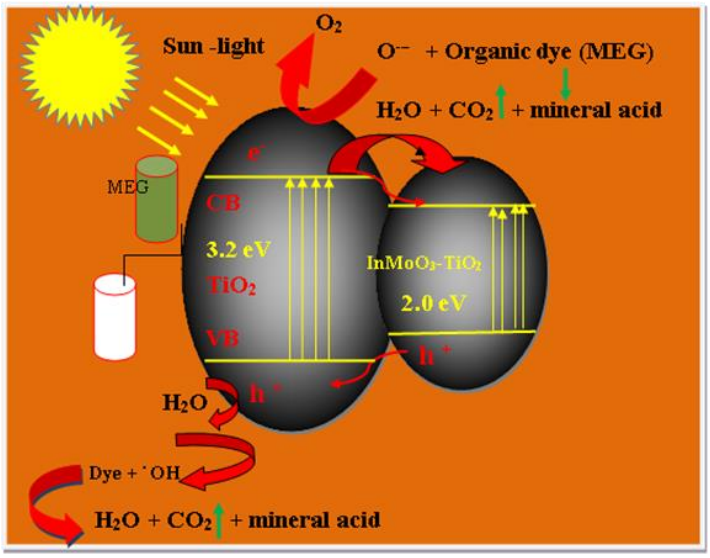

Scheme. 2. $InMoO_3$-doped TiO_2 (IMT)-Photodegradation and Mineralization of MEG under natural sun light irradiation.

3.5. Chemical Oxygen Demand (COD) Analysis

As shown in from Fig.10. 0, 15, 30 and 45 min reduction have been completed. 0, 36, 71 and 97 % of COD reduction is obtained shown in Table.2. This indicates the total mineralization of MEG dye natural sun light reduction. The mineralization is also specific by formation of Calcium carbonate when the evolved gas (CO_2) is passed through calcium hydroxide solution obtained [21].

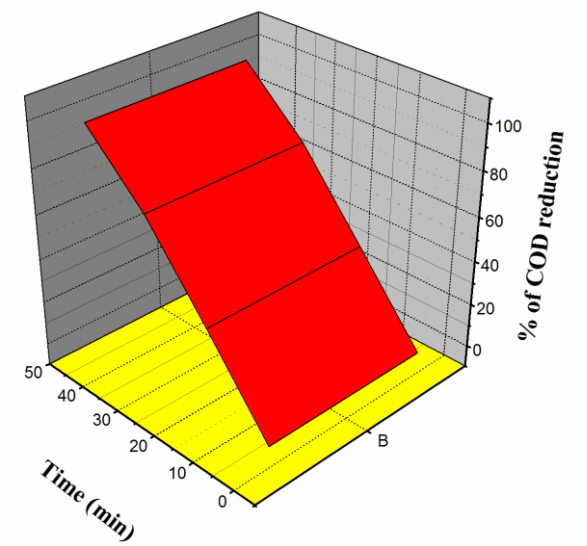

Figure 10. Chemical Oxygen Demand (COD) Analysis of $InMoO_3$-TiO_2 on MEG dye under sun light reduction.

Table.2. COD measurements

Time(min)	% COD reduction
0	0
15	36
30	71
45	97

[MEG] = 1 X 10^{-4} mol L^{-1}; $InMoO_3$-TiO_2 (0.150 g) suspension = 40 mL pH = 7 Solution and air passing with solar-light irradiation.

4. CONCLUSION

Development of Heterostructured $InMoO_3$ doped-TiO_2 nanocomposite material was synthesised by co-precipitation method and sonication technique. It was characterized by XRD, FE-SEM with EDX, HR-TEM analysis. XRD and FT-IR analysis was conformed metal. FE-SEM and HR-TEM image showed the $InMoO_3$ Doped -TiO_2 had spherical shaped structure. EDX spectra revealed the presence of Ti, In, Mo and O in the catalyst. UV–Vis-DRS results demonstrated that the decrease in the direct band gap of $InMoO_3$ -TiO_2 nanomaterial was high photocatalytic activity and chemical oxygen demand (COD) measurements confirmed complete mineralization of the MEG molecule. $InMoO_3$ Doped -TiO_2 material shows superior photocatalytic activity when compared undoped TiO_2 and TiO_2P25 under natural sunlight

irradiation and environmentally friendly. A mechanism proposed Mineralization of MEG under natural sun light irradiation and First-order kinetic study and high quantum yield estimation was obtained. This catalyst was found to stable and reusable.

REFERENCES

[1] Haithem Bel Hadjltaief, Mourad Ben Zina, Maria Elena Galvez, Patrick Da Costa ;Photocatalytic degradation of methyl green dye in aqueous solution over natural clay-supported ZnO–TiO_2 catalysts, Journal of Photochemistry and Photobiology A: Chemistry 2016, 315, 25–33.

[2] J.M. Herrmann, Heterogeneous photocatalysis: fundamentals and applications to the removal of various types of aqueous pollutants, Catal. Today 1999, 53, 115–129.

[3] J. Kamalakkannan, V. L. Chandraboss, S. Prabha and S. Senthilvelan. Advanced construction of Heterostructured InCrO4–TiO2 and its dual properties of greater UVphotocatalytic and antibacterial activity, RSC Adv., 2015, 5, 77000–77013

[4] Jamil, T. S.; Gad-Allah, T. A.; Ghaly, M. Y. Parametric study on phenol photocatalytic degradation under pure visible and solar irradiations by Fe-doped TiO_2. *Desalin. Water Treat.* **2012**, *50*, 264-270.

[5] Xu, T.; Zhang, L.; Cheng, H.; Zhu, Y. Significantly enhanced photocatalytic performance of ZnO via graphene hybridization and the mechanism study. *Appl. Catal. B.* 2011, *101*, 382-387.

[6] Hidalgo, M. C.; Murcia, J. J.; Navio J. A.; and Colon, G. Photodeposition of gold on titanium dioxide for photocatalytic phenol oxidation, *Appl. Catal. A*, **2011**, *397***,** 112-120**.**

[7] Pasini, T.; Piccinini, M.; Blosi, M.; Bonelli, R.; Albonetti, S.; Dimitratos, N.; Lopez J. A. ; Sanchez, Sankar, M.; He, Q.; Kiely, C. J.; Hutchings, G. J.; and Cavani, F. Climate Change Mitigation: Greenhouse Gas Reduction and Biochemicals, *Green Chem.* **2011**, *13*, 2091-2099**.**

[8] Zibin Hai, Nadia EL Kolli, Jiafu Chen and Hynd Remita, Radiolytic synthesis of Au–Cu bimetallic nanoparticles supported on TiO_2: application in photocatalysis, *New J. Chem.* **2014,** *38,* 5279--5286
[9] Khatamian, M.; Alaji, Z. Efficient adsorption-photodegradation of 4-nitrophenol in aqueous solution by using ZnO/HZSM-5 nanocomposites. *Desalination.* **2012**, *286*, 248-253.

[10] Marcý, G.; Augugliaro, V.; Lopez-Munoz, M. J.; Martýn, C.; Palmisano, L.; Rives, V.; Schiavello, M.; Tilley, R. J.D.; Venezia, A. M. Preparation characterization and photocatalytic activity of polycrystalline ZnO/TiO2 systems. 2. Surface and bulk characterization, and 4-
nitrophenol photodegradation in liquid−solid regime. *J. Phys. Chem. B.* **2001**, *105*, 1033-1040.

[11] Papp J.; Soled S.; Dwight K.; Wold A Surface acidity and photocatalytic activity of TiO_2, WO_3/TiO_2, and MoO_3/TiO_2 photocatalysts . *Chem Mater*. **1994**, *6*, 496-500.

[12] Yin, J, Z.; Zou, J,; Ye Yin, J,; Zou, Z,; Ye, J. Photophysical and photocatalytic properties of new photocatalysts $MCrO_4$ (M = Sr, Ba). *Chem. Phys. Lett*. **2003**, 378, 24-28.

[13] Tanmay Ghorai, Niladri Biswas Photodegradation of rhodamine 6G in aqueous solution via $SrCrO_4$ and TiO_2 nano-sphere mixed oxides. *J. Mater. Res. Technol*. **2013**, *2*, 10-17.

[14] E. Haque, J. W. Jun, S. H. Jhung, Adsorptive removal of methyl orange and methylene blue from aqueous solution with a metal-organic framework material, iron terephthalate (MOF-235)
Haz. Mate., **2011**, *185*, 507- 511.

[15]. Balachandran, S.; Prakash, N.; Thirumalai, K.; Muruganandham, M.; Sillanpaa M.; and Swaminathan, M. Facile Construction of Heterostructured $BiVO_4$–ZnO and Its Dual Application of Greater Solar Photocatalytic Activity and Self-Cleaning Property, *Ind. Eng. Chem. Res.*, **2014**, *53*, 8346–8356.

[16] Ge, L.; Xu, M.; Fang, H. Photo-catalytic degradation of methyl orange and formaldehyde by Ag/$InVO_4$–TiO_2 thin films under visible-light irradiation. *J Molecular Catal A: Chemical.* **2006**, *258*, 68-76.

[17] Chandraboss, V. L.; Kamalakkannan, J.; Prabha, S.; and Senthilvelan, S. An efficient removal of methyl violet from aqueous solution by an AC-Bi/ZnO nanocomposite material, RSC Adv. **2015**, *5*, 25857–25869.

[18] Subash, B.; Krishnakumar, R.; Swaminathan M and Shanthi, M. Highly Efficient, Solar Active, and Reusable Photocatalyst: Zr-Loaded Ag−ZnO for Reactive Red 120 Dye Degradation with Synergistic Effect and Dye-Sensitized Mechanism. *Langmuir.* **2013**, 29, 939−949.

[19] Kamalakkannan, J.; Chandraboss, V. L. ; Loganathan, B.; Prabha, S.; Karthikeyan B.; and Senthilvelan, S. $TiInCrO_6$-Nanomaterial Synthesis, Characterization and multi applications, *Appl Nanosci*, **2015**, DOI 10.1007/s13204-015-0474-y.

[20] Balachandran, S.; Gopinathan, S.; Praveen, Velmurugan, R.; and Swaminathan**,** M. Facile fabrication of highly efficient, reusable heterostructured Ag–ZnO–CdO and its twin applications of dye degradation under natural sunlight and self-cleaning, *RSC Adv.* **2014**, *4*, 4353–4362

[21] Subash, B.; Krishnakumar, B.; Velmurugan, R.; Swaminathan M.; and Shanthi, M. Synthesis of Ce co-doped Ag–ZnO photocatalyst with excellent performance for NBB dye degradation under natural sunlight illuminationw*Catal. Sci. Technol.* **2012**, *2*, 2319–2326.

The authors declare no conflict of interest

© 2015 By the Authors; Licensee Borderless Science Publishing, Canada. This is an open access article distributed under the terms and conditions of the Creative Commons Attribution license http://creativecommons.org/licenses/by/3.0